

Supplement of Atmos. Chem. Phys., 20, 2637–2665, 2020
<https://doi.org/10.5194/acp-20-2637-2020-supplement>
© Author(s) 2020. This work is distributed under
the Creative Commons Attribution 4.0 License.



Supplement of

An evaluation of global organic aerosol schemes using airborne observations

Sidhant J. Pai et al.

Correspondence to: Sidhant J. Pai (sidhantp@mit.edu) and Colette L. Heald (heald@mit.edu)

The copyright of individual parts of the supplement might differ from the CC BY 4.0 License.

Simulation	Simulation Periods	Lumped Organic Aerosol Tracers	POA Treatment	SOA Treatment
Simple Scheme		<ul style="list-style-type: none"> EPOA and OPOA (Non-volatile) SOA M-EPOA and M-OPOA 		<p>Non-volatile SOA. Emitted with the following emission factors:</p> <ul style="list-style-type: none"> 1.5% SOA precursor (SOAP) and 1.5% SOA from isoprene 5% SOAP and 5% SOA from monoterpenes and sesquiterpenes, 1.3% SOAP from CO emissions from fire sources 6.9% of CO emissions from anthropogenic combustion sources.
Modified Simple Scheme	2007/03/01 – 2008/08/01 2009/11/01 – 2010/07/01 2011/12/01 – 2012/07/01	<ul style="list-style-type: none"> A-EPOA, A-OPOA and ASOA (Non-volatile anthropogenic OA) F-EPOA, F-OPOA and FSOA (Non-volatile pyrogenic OA) M-EPOA and M-OPOA (Non-volatile marine POA) ISOA (Non-volatile isoprene SOA) TSOA (Non-volatile terpene SOA) 	<p>Non-volatile POA.</p> <p>50% is emitted as fresh hydrophobic OA (EPOA) and 50% is emitted directly as aged hydrophilic OA (OPOA).</p> <p>EPOA is aged to OPOA in the atmosphere with a fixed lifetime of 1 day.</p>	<p>SOAP converts to SOA with a fixed lifetime of 1.15 days.</p> <p>The modified scheme individually simulates SOAP and SOA from each source. The default simple scheme lumps SOAP and SOA from all sources.</p>
Pure VBS Scheme	2012/06/01 – 2014/01/01 2013/09/01 – 2014/02/01 2014/02/01 – 2014/11/01 2015/11/01 – 2016/09/01 2016/08/01 – 2017/03/01	<ul style="list-style-type: none"> EPOA and OPOA ASOA (VBS anthropogenic SOA) ISOA (VBS isoprene SOA) TSOA (VBS terpene SOA) M-EPOA and M-OPOA (Non-volatile marine POA) 	<p>Semi-volatile. 49% is emitted as EPOG₁ with a saturation concentration (C*) of 1646 µg m⁻³ and 51% is emitted as EPOG₂ with C* of 20 µg m⁻³. EPOG₁ and EPOG₂ reversibly partition to EPOA₁ and EPOA₂.</p> <p>EPOG₁ and EPOG₂ are aged in gas-phase via reaction with OH radical to OPOG₁ and OPOG₂ with C* of 16.46 µg m⁻³ and 0.2 µg m⁻³ respectively.</p>	<p>Gas-phase SOA precursors (aromatics, IVOCs, terpenes and isoprene) are oxidized with oxidants OH, O₃ to form alkyl peroxy (RO₂) radicals that react with either HO₂ or NO depending on the NO_x regime.</p> <p>The resulting products are classified based on the origins of their precursors into Anthropogenic SOA (ASOA), Isoprene SOA (ISOA) and Terpene SOA (TSOA), that dynamically partition between the aerosol and gas phases based on their saturation vapor pressures and ambient aerosol concentrations. Aerosol formed from intermediate volatility organic compounds (IVOCs) is modelled using naphthalene as a proxy which, when oxidized, contributes to the ASOA lumped product.</p>
Complex Scheme		<ul style="list-style-type: none"> EPOA and OPOA (Semi-volatile) ASOA (VBS anthropogenic SOA) ISOA (Aqueous isoprene SOA) TSOA (VBS terpene SOA) OrgNit (Organic Nitrates) M-EPOA and M-OPOA (Non-volatile marine POA) 		<p>The Complex scheme builds on VBS framework but replaces VBS isoprene SOA with isoprene-derived OA formed irreversibly from the aqueous phase reactive uptake of isoprene oxidation products. It also includes an explicit formation mechanism for organo-nitrates from isoprene and monoterpene oxidation pathways.</p>

Table S1. A brief description of the various simulations presented in this study

S1. Model Sampling with the ‘Planeflight Diagnostic’

Latitude, longitude and timestamp information was extracted from the aircraft campaign data and used in conjunction with the default GEOS-Chem ‘Planeflight Diagnostic’ to sample the appropriate model gridbox at the appropriate spatial and temporal spot. Model transport timestep was set for 10 minute intervals and chemistry timestep was set at 20 minutes. Diagnostic output from the planeflight sampling was averaged in cases where multiple observations were conducted within the span of a single model timestep within a certain gridbox.

S2. Organic Aerosol in the Complex Scheme

S2.1 Absorptive Partitioning

The complex scheme simulates both primary and secondary OA as semi-volatile using an absorptive partitioning model (Chung and Seinfeld, 2002; Pye et al., 2010), with each class of organic compound (i) associated with a saturation vapor pressure (C_i^*) that determines the fraction of the tracer in both gas and aerosol phase using the following relationship:

$$C_i^* = \frac{[G_i][M_o]}{[A_i]} \quad (S1)$$

$$[M_o] = \sum [A_i] \quad (S2)$$

Where $[G_i]$ and $[A_i]$ are the concentrations of the semi-volatile i in the gas and aerosol phase respectively and $[M_o]$ is the concentration of the particle-phase absorptive material into which the semi-volatile i can partition. The saturation vapor pressure is temperature dependent and is dynamically calculated using the following equation:

$$\frac{C_i^*(T_2)}{C_i^*(T_1)} = \frac{T_2}{T_1} \exp\left(\frac{\Delta H_i}{R} \left(\frac{1}{T_2} - \frac{1}{T_1}\right)\right) \quad (S3)$$

An enthalpy of vaporization of 50 kJ mol^{-1} is assumed to estimate C^* over a range of ambient temperatures.

S2.2 POA

49% of POA is emitted as EPOG₁ with a saturation concentration (C^*) of $1646 \mu\text{g m}^{-3}$ and 51% is emitted as EPOG₂ with C^* of $20 \mu\text{g m}^{-3}$. EPOG₁ and EPOG₂ reversibly partition to EPOA₁ and EPOA₂. EPOG₁ and EPOG₂ are aged in gas-phase via reaction with the OH radical (k_{OH} of 2×10^{11}) to OPOG₁ and OPOG₂ with C^* of $16.46 \mu\text{g m}^{-3}$ and $0.2 \mu\text{g m}^{-3}$ and respectively (Grieshop et al., 2009; Pye et al., 2010)

S2.3 SOA from Aromatic VOCs and Terpenes (Pye et al., 2010)

Gas-phase anthropogenic and select biogenic VOCs are oxidized (with oxidants - OH, O₃) to form alkyl peroxy (RO₂) radicals that then react with either HO₂ or NO to form second-generation aerosol products depending on the NO_x regime – with high and low NO_x yields and partitioning coefficients based on experimental fits from laboratory studies (See Table 1 in Pye et al., 2010). These second-generation products are assigned volatilities with C^* ranging from 0.1, 1, 10 and $100 \mu\text{g m}^{-3}$ and partition between aerosol and gas phase based on the equations listed above. This framework is referred to as the ‘Volatility Basis Set’ (VBS) and its implementation in the GEOS-Chem model is outlined in Pye et al. (2010). Aromatic VOCs are simulated using benzene, toluene and xylene, which are oxidized to form 4 lumped semi-volatile products. Terpenoids (monoterpenes and sesquiterpenes) are also oxidized to form 4 lumped products with C^* of 0.1, 1, 10, 100. A detailed overview of the second-generation yields can be found in Pye et al. (2010).

S2.4 SOA from IVOCs (Pye et al., 2010)

Intermediate Volatility Organic Compounds (IVOCs) such as alcohols and phenols have been shown to form SOA on oxidation (Chan et al., 2009; Pye et al., 2010). Phenol and substituted phenol compounds have been shown to be major

contributors to IVOC emissions (Schauer et al., 2001) and exhibit similar behavior to naphthalene in terms of their aerosol yields. Thus, IVOCs are represented as a naphthalene-like surrogate (Pye et al., 2010) and assumed to form SOA in accordance with the parameters derived from the chamber studies of Chan et al. 2009. Global IVOC emissions are uncertain but are assumed to have the spatial distribution of naphthalene. For biofuel and biomass burning, naphthalene emissions are approximated using CO as a proxy, with an emission ratio of 0.0602 and 0.0701 mmol naphthalene / mol CO for biomass and biofuel burning respectively (Andreae and Merlet, 2001; Pye et al., 2010). Anthropogenic IVOC emissions are estimated from the CEDS Inventory and were scaled from benzene emissions using the same scale factors used by Pye et al. (2010).

S2.5 Explicit Mechanism for SOA from Isoprene (Marais et al., 2016)

Isoprene oxidation occurs through an explicit mechanism outlined in Marais et al. (2016). In this mechanism most of the isoprene undergoes oxidation via OH to form a peroxy radical which in turn reacts with HO₂, NO, other peroxy radicals (RO₂) or undergoes isomerization. The HO₂ reaction pathway leads to the formation of hydroxyhydroperoxides (ISOPPOOH) that are oxidized by OH to isoprene epoxydiol (IEPOX) and several low-volatility products, that are represented in the model as the C₅-LVOC lumped product which, despite its name is assumed to be non-volatile. The high-NO_x (NO) pathway results in C₅ hydroxy carbonyls, methyl vinyl ketone, methacrolein, and first-generation isoprene nitrates (ISOPN). The first three products react with OH to produce glyoxal (GLYX) and methylglyoxal (MGLY). ISOPN is oxidized with OH to form dihydroxy dinitrates (DHDN) and IEPOX. Reaction of the peroxy radical with RO₂ is a minor pathway that ultimately leads to the formation of C₄ hydroxyepoxides (MEPOX) as well as GLYX and MGLY. Isomerization is a similarly minor pathway that leads to the formation of a hydroperoxyaldehyde that forms GLYX and MGLY when photolyzed. IEPOX also forms GLYX and MGLY on oxidation with OH.

In addition to the processes above, isoprene also undergoes ozonolysis and reaction with NO₃, forming MGLY and second generation hydroxy-nitrates (NT-ISOPN). IEPOX, GLYX, MGLY, C₅-LVOC, MEPOX, ISOPN, DHDN, NT-ISOPN form non-volatile aerosols through an irreversible aqueous reactive uptake parametrization. A more detailed overview of the relevant mechanism, yields, reaction rates, branching ratios and uptake coefficients can be found in Marais et al. (2016).

S2.6 Explicit Mechanism for Organo-nitrates from Terpenes (Fisher et al., 2016)

Terpene species also form aerosol-phase organo-nitrates through an explicit mechanism defined in Fisher et al. (2016). During the day, terpene precursors react with OH to form peroxy radicals which then react with NO to form first generation monoterpene nitrates with a yield of 18%. These are then further oxidized to form second-generation monoterpene nitrates. At night, these terpenes react with NO₃ to form nitrooxy peroxy radicals that either decompose or form a more stable organo-nitrate with a predefined branching ratio based on the precursor. Formation of non-volatile aerosol from gas-phase organo-nitrate is modelled using an irreversible reactive uptake parameterization, followed by particle-phase hydrolysis. A more detailed overview of the relevant mechanism, yields, reaction rates, branching ratios and uptake coefficients can be found in Fisher et al. (2016).

S3. OA Loss Processes: Dry and Wet Deposition

Organic Aerosol is deposited from the atmosphere through both wet deposition and dry deposition. Dry deposition is estimated using a parametrization described in Zhang et al. (2001) that calculates particle deposition velocities as a function of particle size, density and relevant meteorology and accounts for turbulent transfer, Brownian diffusion, impaction, interception, gravitational settling and particle rebound. Particle diameter and density is assumed to be 0.5 μm and 1500 kg m^{-3} respectively. Deposition velocities are calculated using the following relationship:

$$V_d = V_g + \frac{1}{(R_a + R_s)} \quad (\text{S4})$$

where V_g is the gravitational settling velocity, R_a is the aerodynamic resistance above the canopy and R_s is the surface resistance. A more detailed derivation of the individual terms can be found in Section 2 of Zhang et al. (2001).

Wet deposition occurs through two processes – ‘Rainout’ defined by in-cloud scavenging and ‘Washout’ defined by below-cloud scavenging. Rainout scavenges aerosols efficiently and is sensitive to the fraction of the grid-box that experiences precipitation. This fraction is calculated online using the grid-scale precipitation formation rate (Q_k), cloud condensed water content (L), the duration of the model timestep, the duration of precipitation over the time step (T_c) and rate constant for conversion of cloud water to precipitation (C_1). See Liu et al. (2001) for more details. Below-cloud scavenging is calculated using a washout rate applied to the precipitation fraction described above. The model also simulates the release of aerosol during the re-evaporation of precipitation as it falls to the ground. Scavenging of aerosols is also modelled from cloud updrafts in moist convection and the fraction of aerosol tracer scavenged by the convective precipitation in the updraft is defined by the following relationship:

$$Conv_{frac} = 1 - e^{-\alpha\Delta z} \quad (\text{S5})$$

where Δz is the thickness of the convective column and α is the scavenging efficiency.

The fraction of gas-phase OA precursors wet deposited is dictated by the liquid to gas ratio for a grid-box at any given timestep. For a soluble gas ‘i’, this ratio is calculated based on the following relationship:

$$\frac{C_{i,L}}{C_{i,G}} = K_i^* * L * R * T \quad (\text{S6})$$

where K_i^* is the effective Henry’s law constant that is calculated using the van’t Hoff equation (Jacob et al., 2000), L is the cloud liquid water content, R is the ideal gas constant and T is the local temperature. Each organic gas-phase species has an associated Henry’s law solubility constant (in M atm^{-1}), volatility constant (in K) and pH correction factor which is defined in the GEOS-Chem species database. A detailed overview of the wet deposition scheme can be found in Jacob et al. (2000), Liu et al. (2001) and Amos et al. (2012).

S4. Nomenclature: Oxygenated Primary Organic Aerosol (OPOA) vs Secondary Organic Aerosol (SOA)

The OPOA product is formed by the oxidation of EPOA. In the simple scheme, this process is approximated by a fixed lifetime of 1 day with no direct dependence on oxidant concentrations. In the complex scheme, EPOA is oxidized with OH to form oxygenated primary organic vapors. Many previous studies in the literature have represented the aerosol formed from these vapors as Oxygenated POA (Donahue et al., 2009; Pye et al., 2010; Shrivastava et al., 2008)

but the nomenclature has been the topic of some contention, with other studies preferring to use the terminology of Secondary Organic Aerosol (SOA) to represent this aerosol product (Hayes et al., 2015; Murphy et al., 2014). For the purpose of this study we have chosen to refer to aerosol resulting from the oxidation of primary organic matter that is already semi-volatile as OPOA and reserve the term SOA exclusively for aerosol formed from the oxidation of volatile organic vapors. We are further motivated to maintain these labels given that this is how they are described in the GEOS-Chem model and the relevant model paper (Pye et al., 2010). We have separated the OPOA contribution and discussion whenever possible in this study to allow the reader to interpret the results as desired.

Campaign	Organic Aerosol	NO _x	Isoprene	CO
ARCPAC	C-ToF-AMS (A.M. Middlebrook)	NOAA NO_yO₃ (T.B. Ryerson)	PTR-MS (J.A. de Gouw, C. Warneke)	VUV Resonance Fluorescence (J.S. Holloway)
ARCTAS	HR-ToF-AMS (J.L. Jimenez)	NCAR 4 channel Chemiluminescence (A.J. Weinheimer, F.M. Flocke, D.J. Knapp, D.D. Montzka, I.B. Pollack)	TOGA (E. Apel, R. Hornbrook)	DACOM (G.S. Diskin, G. Sachse)
EUCAARI	C-ToF-AMS (H. Coe)			
OP3	C-ToF-AMS (H. Coe)			
CalNex	C-ToF-AMS (A.M. Middlebrook)	NOAA NO_yO₃ (T.B. Ryerson, I.B. Pollack)	PTR-MS (J.A. de Gouw, C. Warneke)	VUV Resonance Fluorescence (J.S. Holloway)
DC3	HR-ToF-AMS (J.L. Jimenez)	NOAA NO_yO₃ (T.B. Ryerson, I.B. Pollack)	PTR-MS (T. Mikoviny, A. Wisthaler)	DACOM (G.S. Diskin, G. Sachse)
SENEX	C-ToF-AMS (A.M. Middlebrook)	NOAA NO_yO₃ (T.B. Ryerson, I.B. Pollack)	PTR-MS (M. Graus)	VUV Resonance Fluorescence (J.S. Holloway)
SEAC4RS	HR-ToF-AMS (J.L. Jimenez)	NOAA NO_yO₃ (T.B. Ryerson, I.B. Pollack, J. Peischl)	WAS (D.R. Blake)	DACOM (G.S. Diskin, G. Sachse)
GoAmazon	HR-ToF-AMS (J.E. Shilling)		PTR-MS (J.E. Shilling)	Los Gatos ICOS Analyzer (S.R. Springston)
FRAPPE	C-ToF-mAMS (R. Bahreini)	NCAR 2-channel Chemiluminescence (A.J. Weinheimer, D.D. Montzka)	TOGA (E. Apel, R. Hornbrook)	Aero-Laser VUV Fluorescence (T.L. Campos and F.M. Flocke)
KORUS-AQ	HR-AMS (J.L. Jimenez, P. Campuzano-Jost)	NCAR 4-channel Chemiluminescence (A.J. Weinheimer, D.D. Montzka)	PTR-MS (P. Eichler, L. Kaser, T. Mikoviny, M. Müller, A. Wisthaler)	DACOM (G.S. Diskin, S.E. Pusede)
ATom	HR-ToF-AMS (J.L. Jimenez)	NOAA NO_yO₃ (T.B. Ryerson, J. Peischl, C. Thompson)	TOGA (E. Apel, R. Hornbrook)	QCLS (B.C. Daube, S.C. Wofsy, R. Commane, E. Kort)

Table S2. An overview of the instrumentation and associated primary investigators for the organic aerosol and trace gas observations used in this analysis.

Nitrogen oxides were measured using photolysis rates and NO/O₃ chemiluminescence techniques (Ryerson et al., 2000), carbon monoxide levels were measured using a Differential Absorption Carbon monOxide Measurement (DACOM) instrument (Sachse et al., 1987) or a VUV resonance fluorescence approach (Gerbig et al., 1999), isoprene concentrations were observed using a Proton Transfer Reaction Mass Spectrometer (de Gouw and Warneke, 2007), a Trace Organic Gas Analyzer (Apel et al., 2010) or a whole air sampling approach (Colman et al., 2001) and sulfate aerosol loadings were measured using an AMS.

Regime	Description	Percentage of Dataset	Mean OA	Median OA	Std. Dev. OA	Mean Isoprene	Mean NO _x	Mean CO
A	Dominant anthropogenic influence	39.1%	1.9	0.6	3.2	0.05	0.96	144
F	Dominant pyrogenic influence	7.3%	4.5	2.7	5.3	0.13	0.17	151
B	Dominant biogenic influence	3.6%	3.1	2.6	2.6	1.46	0.16	122
AF	Anthropogenic and pyrogenic influence	6.8%	3.8	1.6	5.0	0.05	0.80	160
AB	Anthropogenic and biogenic influence	14.0%	4.1	2.7	4.0	0.60	0.35	115
AFB	No dominant influence from any one source category.	10.1%	3.2	2.5	2.9	0.10	0.38	115
R	Remote / clean (concentrations under 0.2 µg / sm ³)	19.1%	0.1	0.1	0.3	0.05	0.08	71
Aggregate			2.4	0.7	3.6	0.24	0.55	126

Table S3. An overview of the different regimes. Statistics (mean, median, standard deviation) are listed for the observational data categorized into the individual regimes. OA data is in units of µg sm⁻³. Mean observations for isoprene, nitrogen oxides and carbon monoxide are in units of parts per billion (ppb).

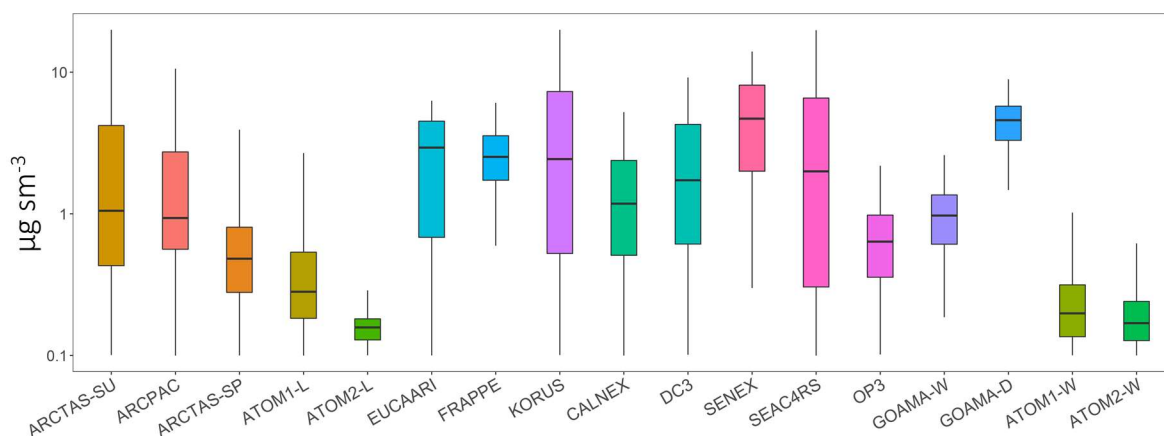


Figure S1. Distribution in the observed organic aerosol concentrations for each campaign. The boxes denote the 25th and 75th percentile of the distribution, while the whiskers denote the 5th and 95th percentile. Observations represented here have been filtered and averaged to the model timestep. The bars are colored by campaign. Refer to Section 3 for more details.

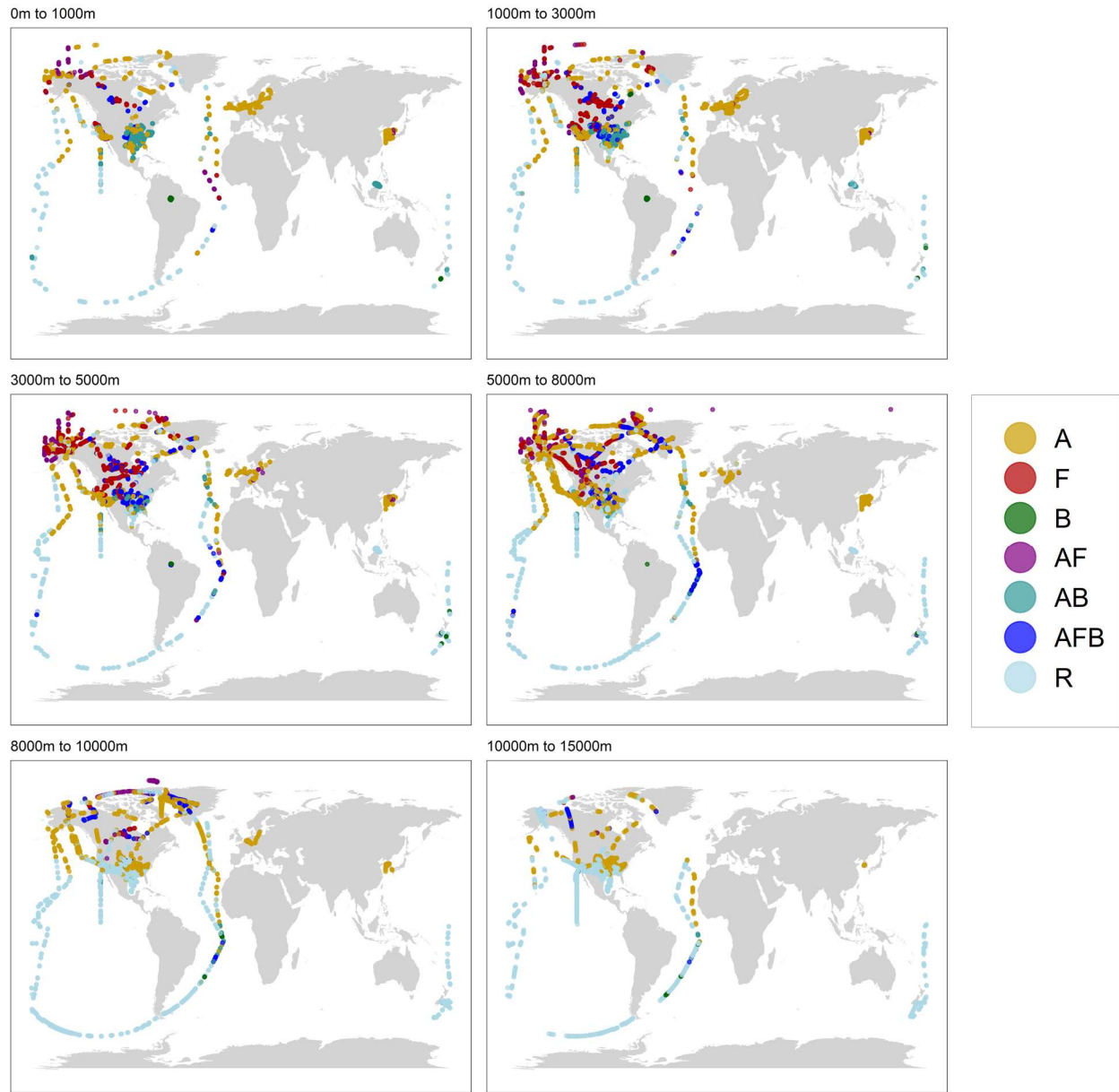


Figure S2. Flight tracks colored by regime type and differentiated by altitude. The Regimes are as follows – Anthropogenic (A), Pyrogenic (F), Biogenic (B), Anthropogenic + Pyrogenic (AF), Anthropogenic + Biogenic (AB), Mixed (AFB) and Remote / Marine (R). Refer to Sect. 3 for details on model sampling and averaging.

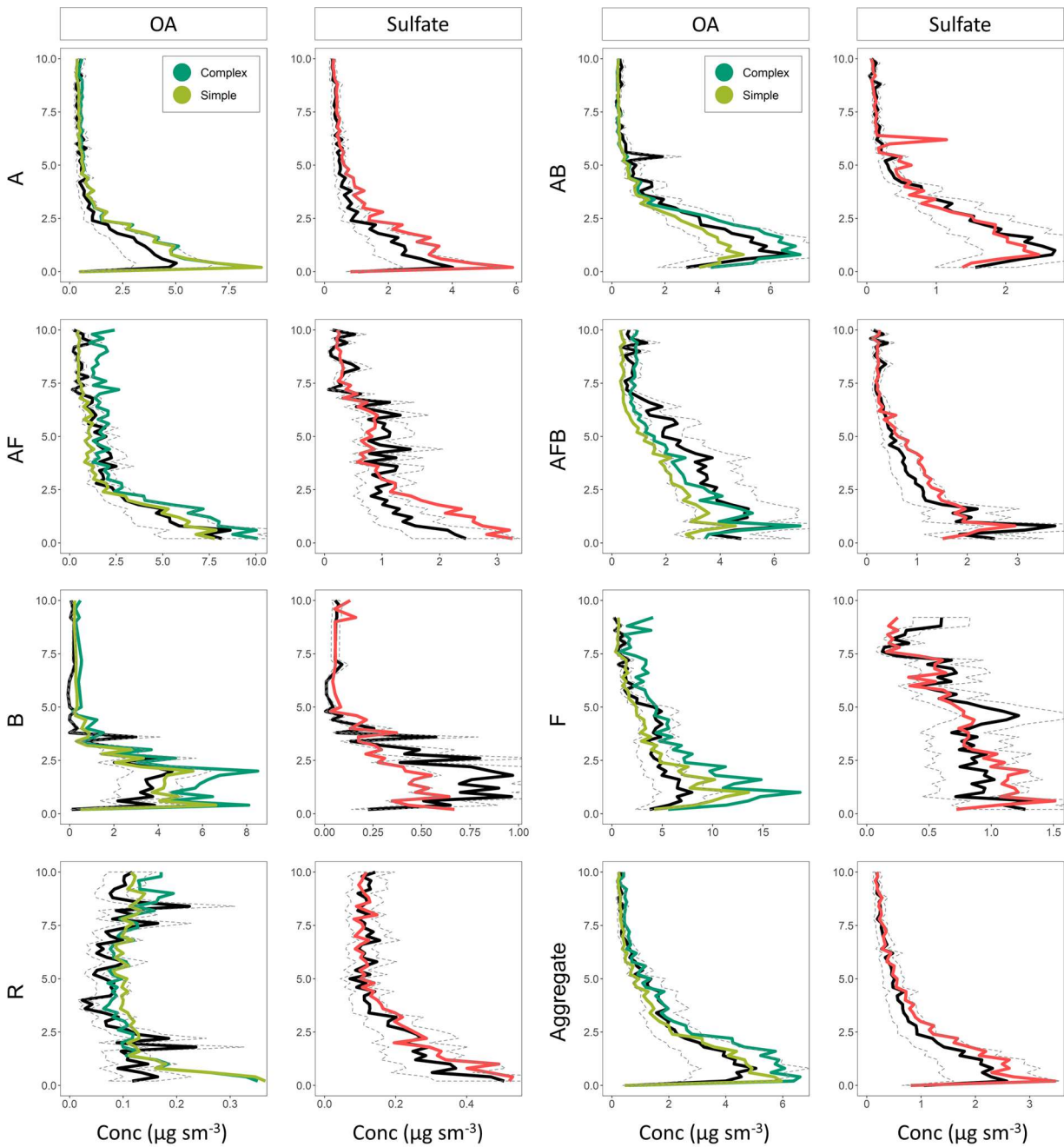


Figure S3. Mean vertical profiles (in km) for the observed and simulated OA and sulfate across the different regimes. The profiles are binned at 200m intervals. Observations are in black. For the OA, the complex scheme is in dark green while the simple scheme is in light green. Model sulfate is in red.

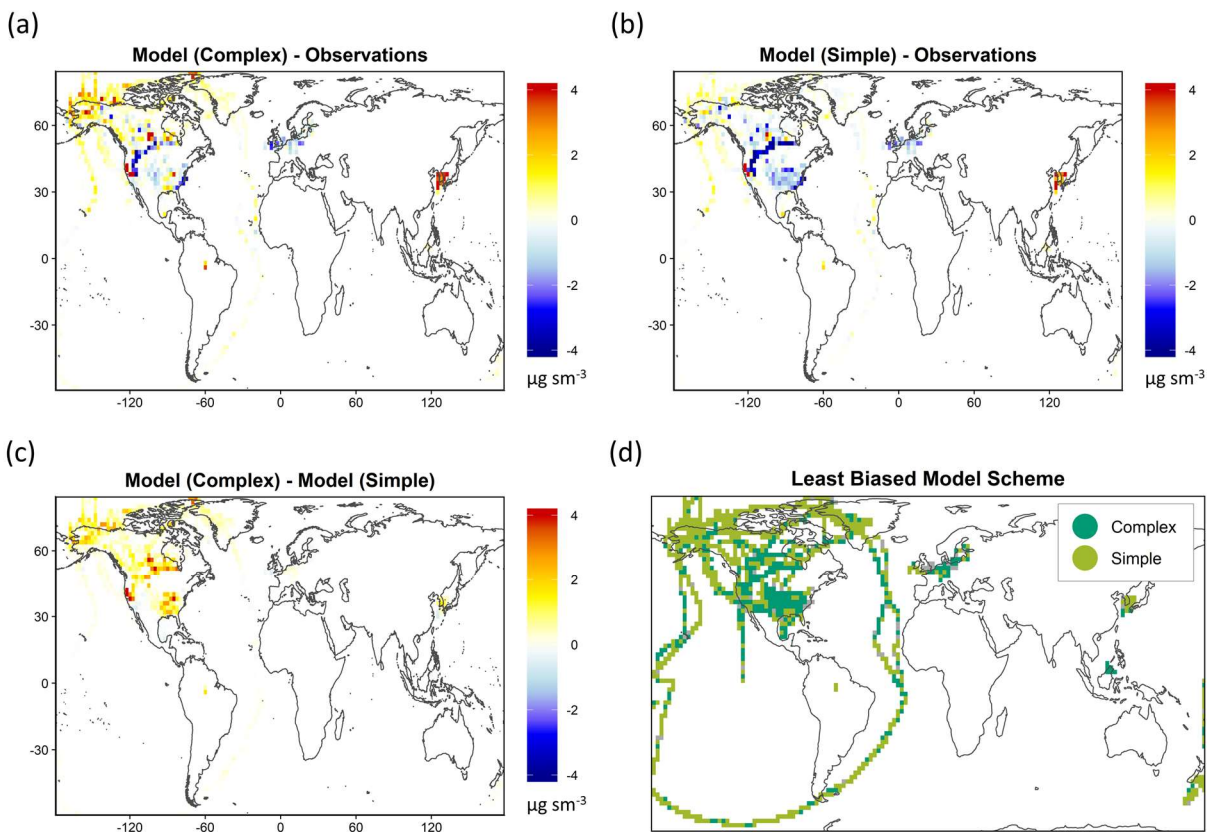


Figure S4. A comparison of the simulated OA loadings averaged by grid-box over the vertical dimension. Panel (d) provides an overview of the column-averaged ‘best fit’ scheme based on the ability to minimize the mean bias.

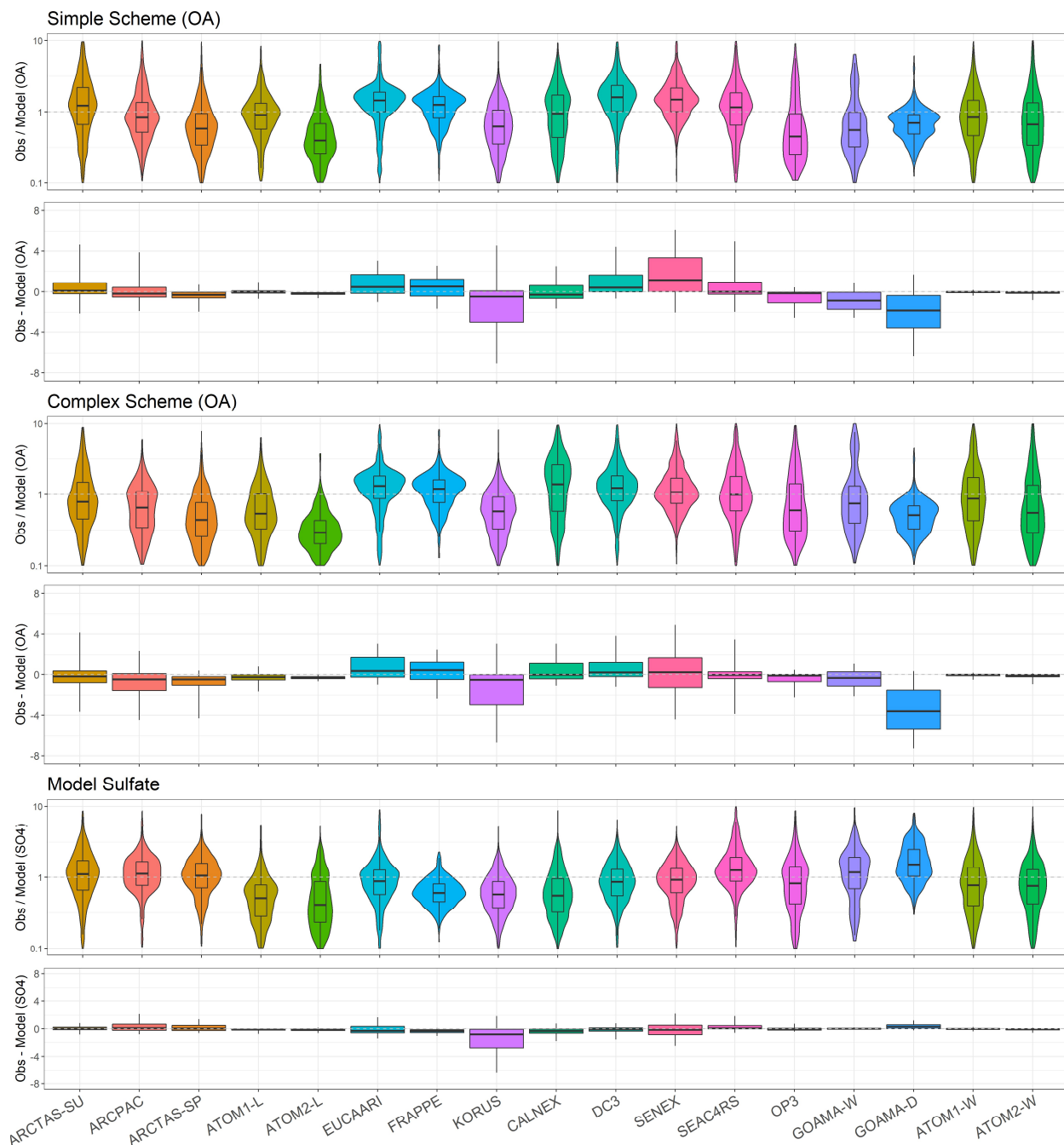


Figure S5. Distribution in the ratio and bias between the observed and modelled organic aerosol concentrations for each model scheme across the 17 campaigns. The boxes denote the 25th and 75th percentile of the distribution, while the whiskers denote the 5th and 95th percentile. The ratio plots have been overlaid with violin plots describing the entire distribution. The box and ratio plots are colored by campaign.

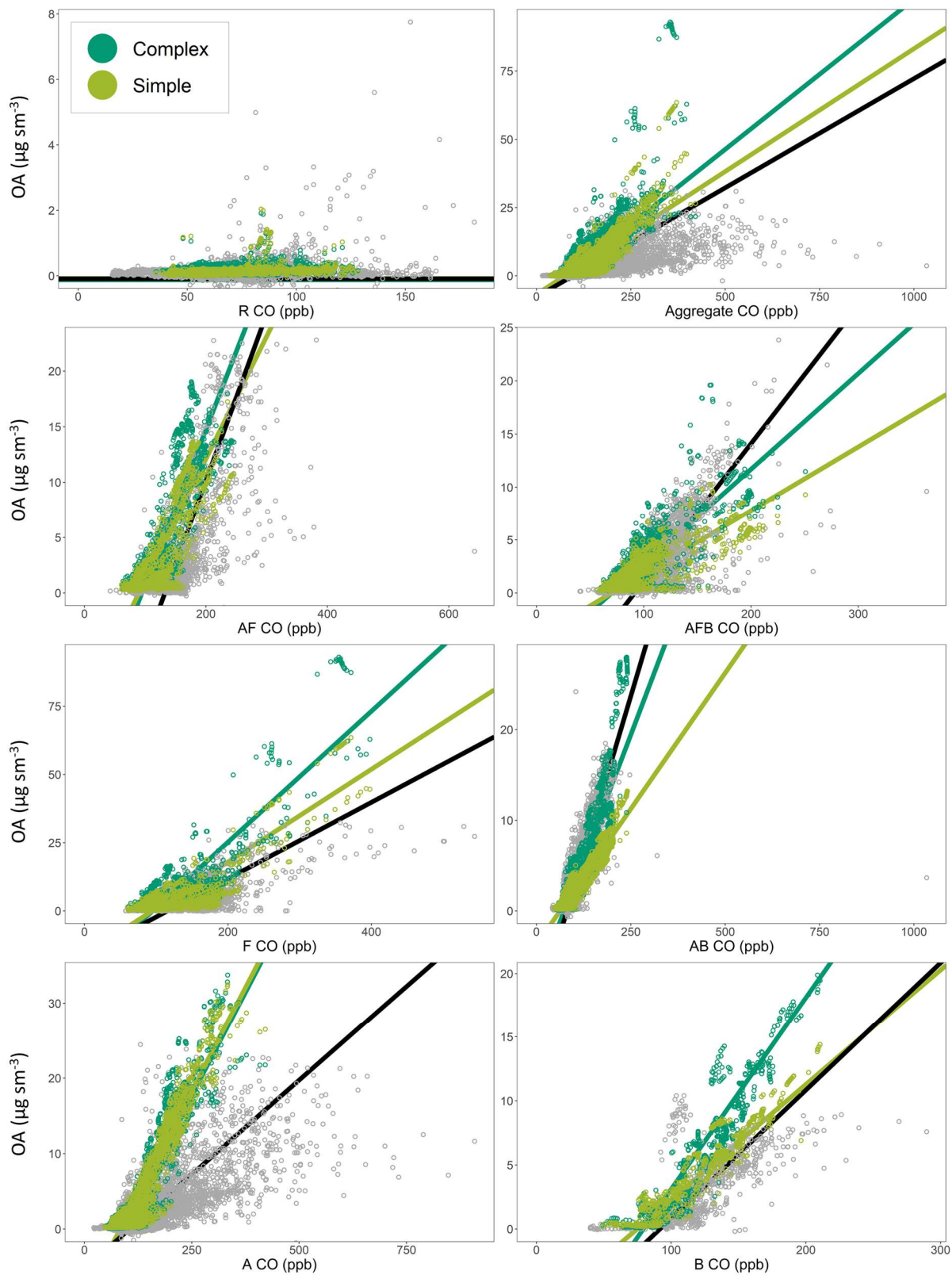


Figure S6. Comparison of complex (dark green), simple (light green) and observed (grey) organic aerosol to carbon monoxide.

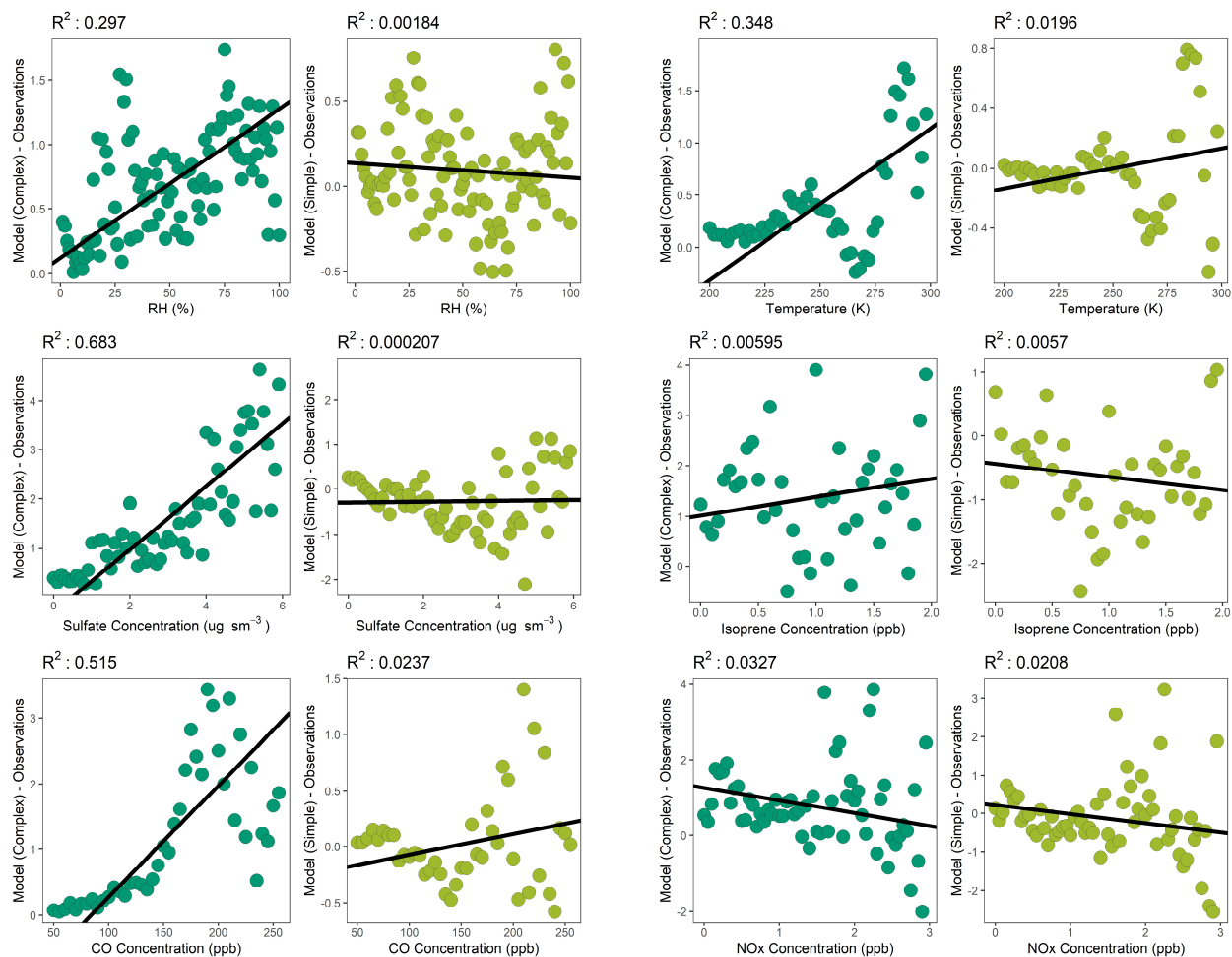


Figure S7. A comparison of model-observation OA bias and binned observations for a) relative humidity, b) Temperature, c) Sulfate, d) Isoprene, e) CO and f) NO_x for the complex (left panels – dark green) and simple (right panels – light green) schemes across the aggregate dataset. The best fit line is shown in black.

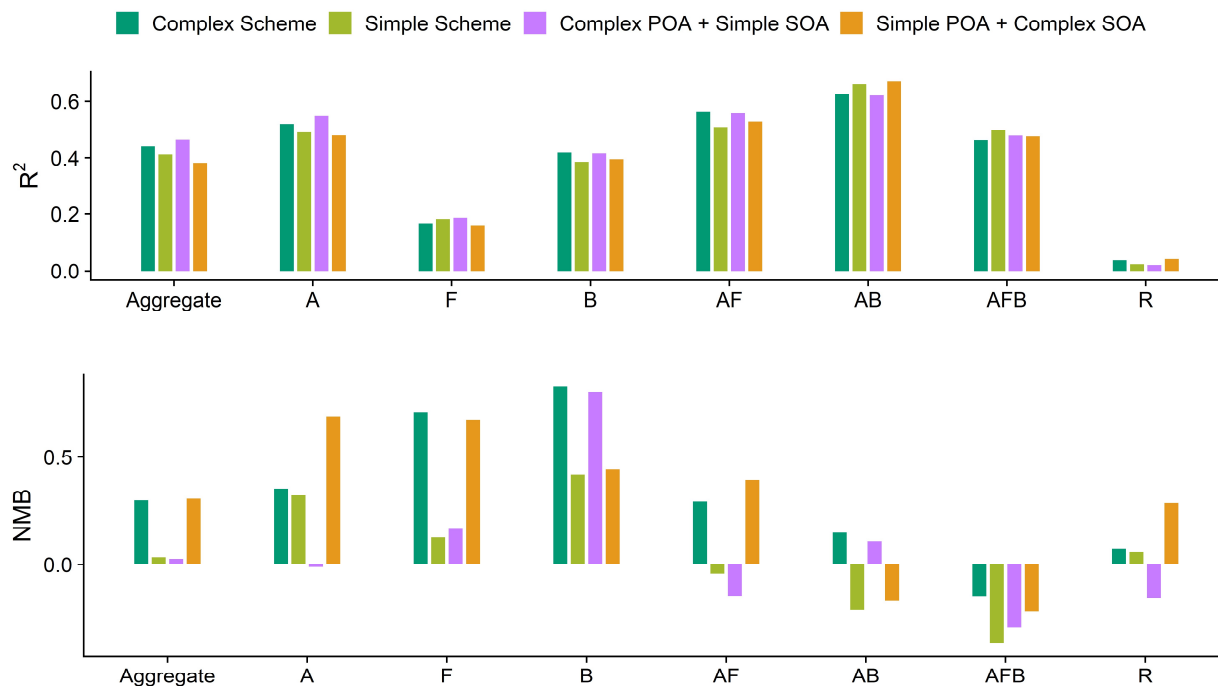


Figure S8. A statistical evaluation of the OA model skill for the complex and simple schemes against a modified treatment that interchanges the POA and SOA from both schemes.

References

- Amos, H. M., Jacob, D. J., Holmes, C. D., Fisher, J. A., Wang, Q., Yantosca, R. M., Corbitt, E. S., Galarneau, E., Rutter, A. P., Gustin, M. S., Steffen, A., Schauer, J. J., Graydon, J. A., Louis, V. L. St., Talbot, R. W., Edgerton, E. S., Zhang, Y. and Sunderland, E. M.: Gas-particle partitioning of atmospheric Hg(II) and its effect on global mercury deposition, *Atmospheric Chem. Phys.*, 12, 591–603, doi:10.5194/acp-12-591-2012, 2012.
- Andreae, M. O. and Merlet, P.: Emission of trace gases and aerosols from biomass burning, *Glob. Biogeochem. Cycles*, 15(4), 955–966, doi:10.1029/2000GB001382, 2001.
- Apel, E. C., Emmons, L. K., Karl, T., Flocke, F., Hills, A. J., Madronich, S., Lee-Taylor, J., Fried, A., Weibring, P., Walega, J., Richter, D., Tie, X., Mauldin, L., Campos, T., Weinheimer, A., Knapp, D., Sive, B., Kleinman, L., Springston, S., Zaveri, R., Ortega, J., Voss, P., Blake, D., Baker, A., Warneke, C., Welsh-Bon, D., de Gouw, J., Zheng, J., Zhang, R., Rudolph, J., Junkermann, W. and Riemer, D. D.: Chemical evolution of volatile organic compounds in the outflow of the Mexico City Metropolitan area, *Atmospheric Chem. Phys.*, 10, 2353–2375, doi:https://doi.org/10.5194/acp-10-2353-2010, 2010.
- Chan, A. W. H., Kautzman, K. E., Chhabra, P. S., Surratt, J. D., Chan, M. N., Crouse, J. D., Kürten, A., Wennberg, P. O., Flagan, R. C. and Seinfeld, J. H.: Secondary organic aerosol formation from photooxidation of naphthalene and alkylnaphthalenes: implications for oxidation of intermediate volatility organic compounds (IVOCs), *Atmospheric Chem. Phys.*, 9(9), 3049–3060, doi:https://doi.org/10.5194/acp-9-3049-2009, 2009.
- Chung, S. H. and Seinfeld, J. H.: Global distribution and climate forcing of carbonaceous aerosols, *J. Geophys. Res.*, 107(D19), doi:10.1029/2001JD001397, 2002.

Colman, J. J., Swanson, A. L., Meinardi, S., Sive, B. C., Blake, D. R. and Rowland, F. S.: Description of the Analysis of a Wide Range of Volatile Organic Compounds in Whole Air Samples Collected during PEM-Tropics A and B, *Anal. Chem.*, 73(15), 3723–3731, doi:10.1021/ac010027g, 2001.

Donahue, N. M., Robinson, A. L. and Pandis, S. N.: Atmospheric organic particulate matter: From smoke to secondary organic aerosol, *Atmos. Environ.*, 43(1), 94–106, doi:10.1016/j.atmosenv.2008.09.055, 2009.

Fisher, J. A., Jacob, D. J., Travis, K. R., Kim, P. S., Marais, E. A., Chan Miller, C., Yu, K., Zhu, L., Yantosca, R. M., Sulprizio, M. P., Mao, J., Wennberg, P. O., Crouse, J. D., Teng, A. P., Nguyen, T. B., Clair, J. M. S., Cohen, R. C., Romer, P., Nault, B. A., Wooldridge, P. J., Jimenez, J. L., Campuzano-Jost, P., Day, D. A., Hu, W., Shepson, P. B., Xiong, F., Blake, D. R., Goldstein, A. H., Misztal, P. K., Hanisco, T. F., Wolfe, G. M., Ryerson, T. B., Wisthaler, A. and Mikoviny, T.: Organic nitrate chemistry and its implications for nitrogen budgets in an isoprene- and monoterpene-rich atmosphere: constraints from aircraft (SEAC⁴RS) and ground-based (SOAS) observations in the Southeast US, *Atmospheric Chem. Phys.*, 16(9), 5969–5991, doi:https://doi.org/10.5194/acp-16-5969-2016, 2016.

Gerbig, C., Schmitgen, S., Kley, D., Volz-Thomas, A., Dewey, K. and Haaks, D.: An improved fast-response vacuum-UV resonance fluorescence CO instrument, *J. Geophys. Res. Atmospheres*, 104(D1), 1699–1704, doi:10.1029/1998JD100031, 1999.

de Gouw, J. and Warneke, C.: Measurements of volatile organic compounds in the earth's atmosphere using proton-transfer-reaction mass spectrometry, *Mass Spectrom. Rev.*, 26(2), 223–257, doi:10.1002/mas.20119, 2007.

Grieshop, A. P., Logue, J. M., Donahue, N. M. and Robinson, A. L.: Laboratory investigation of photochemical oxidation of organic aerosol from wood fires 1: measurement and simulation of organic aerosol evolution, *Atmospheric Chem. Phys.*, 9(4), 1263–1277, doi:https://doi.org/10.5194/acp-9-1263-2009, 2009.

Hayes, P. L., Carlton, A. G., Baker, K. R., Ahmadov, R., Washenfelder, R. A., Alvarez, S., Rappenglück, B., Gilman, J. B., Kuster, W. C., de Gouw, J. A., Zotter, P., Prévôt, A. S. H., Szidat, S., Kleindienst, T. E., Offenberg, J. H., Ma, P. K. and Jimenez, J. L.: Modeling the formation and aging of secondary organic aerosols in Los Angeles during CalNex 2010, *Atmospheric Chem. Phys.*, 15(10), 5773–5801, doi:10.5194/acp-15-5773-2015, 2015.

Jacob, D. J., Liu, H., Mari, C. and Yantosca, R. M.: Harvard wet deposition scheme for GMI, , 6, 2000.

Liu, H., Jacob, D. J., Bey, I. and Yantosca, R. M.: Constraints from ²¹⁰Pb and ⁷Be on wet deposition and transport in a global three-dimensional chemical tracer model driven by assimilated meteorological fields, *J. Geophys. Res. Atmospheres*, 106(D11), 12109–12128, doi:10.1029/2000JD900839, 2001.

Marais, E. A., Jacob, D. J., Jimenez, J. L., Campuzano-Jost, P., Day, D. A., Hu, W., Krechmer, J., Zhu, L., Kim, P. S., Miller, C. C., Fisher, J. A., Travis, K., Yu, K., Hanisco, T. F., Wolfe, G. M., Arkinson, H. L., Pye, H. O. T., Froyd, K. D., Liao, J. and McNeill, V. F.: Aqueous-phase mechanism for secondary organic aerosol formation from isoprene: application to the southeast United States and co-benefit of SO₂ emission controls, *Atmospheric Chem. Phys.*, 16(3), 1603–1618, doi:10.5194/acp-16-1603-2016, 2016.

Murphy, B. N., Donahue, N. M., Robinson, A. L. and Pandis, S. N.: A naming convention for atmospheric organic aerosol, *Atmospheric Chem. Phys.*, 14(11), 5825–5839, doi:10.5194/acp-14-5825-2014, 2014.

Pye, H. O. T., Chan, A. W. H., Barkley, M. P. and Seinfeld, J. H.: Global modeling of organic aerosol: the importance of reactive nitrogen (NO_x and NO₃), *Atmospheric Chem. Phys.*, 10(22), 11261–11276, doi:10.5194/acp-10-11261-2010, 2010.

Ryerson, T. B., Williams, E. J. and Fehsenfeld, F. C.: An efficient photolysis system for fast-response NO₂ measurements, *J. Geophys. Res. Atmospheres*, 105(D21), 26447–26461, doi:10.1029/2000JD900389, 2000.

Sachse, G. W., Hill, G. F., Wade, L. O. and Perry, M. G.: Fast-response, high-precision carbon monoxide sensor using a tunable diode laser absorption technique, *J. Geophys. Res. Atmospheres*, 92(D2), 2071–2081, doi:10.1029/JD092iD02p02071, 1987.

Schauer, J. J., Kleeman, M. J., Cass, G. R. and Simoneit, B. R. T.: Measurement of Emissions from Air Pollution Sources. 3. C1–C29 Organic Compounds from Fireplace Combustion of Wood, *Environ. Sci. Technol.*, 35(9), 1716–1728, doi:10.1021/es001331e, 2001.

Shrivastava, M. K., Lane, T. E., Donahue, N. M., Pandis, S. N. and Robinson, A. L.: Effects of gas particle partitioning and aging of primary emissions on urban and regional organic aerosol concentrations, *J. Geophys. Res.*, 113(D18), D18301, doi:10.1029/2007JD009735, 2008.

Zhang, L., Gong, S., Padro, J. and Barrie, L.: A size-segregated particle dry deposition scheme for an atmospheric aerosol module, *Atmos. Environ.*, 35(3), 549–560, doi:10.1016/S1352-2310(00)00326-5, 2001.